NUREG/CR-3980 Vol. II
ANL-84-61 Vol. II

NUREG/CR-3980 Vol. II
ANL-84-61 Vol. II

LIGHT-WATER-REACTOR SAFETY FUEL SYSTEMS RESEARCH PROGRAMS: QUARTERLY PROGRESS REPORT

April – June 1984

ARGONNE NATIONAL LABORATORY, ARGONNE, ILLINOIS
Operated by THE UNIVERSITY OF CHICAGO

Prepared for the Office of Nuclear Regulatory Research
U. S. NUCLEAR REGULATORY COMMISSION
under Interagency Agreement DOE 40-550-75

Argonne National Laboratory, with facilities in the states of Illinois and Idaho, is owned by the United States government, and operated by The University of Chicago under the provisions of a contract with the Department of Energy.

NUREG/CR-3980 Vol. II
ANL-84-61 Vol. II

Distribution
Code: R3

ARGONNE NATIONAL LABORATORY
9700 South Cass Avenue
Argonne, Illinois 60439

LIGHT-WATER-REACTOR SAFETY FUEL SYSTEMS RESEARCH PROGRAMS: QUARTERLY PROGRESS REPORT

April—June 1984

Date Published: February 1985

Previous reports in this series

ANL-83-85 Vol. II	April—June 1983
ANL-83-85 Vol. III	July—September 1983
ANL-83-85 Vol. IV	October—December 1983
ANL-84-61 Vol. I	January—March 1984

Prepared for the Division of Accident Evaluation
Office of Nuclear Regulatory Research
U. S. Nuclear Regulatory Commission
Washington, D. C. 20555
Under Interagency Agreement DOE 40-550-75

NRC FIN Nos. A2016 and A2017

LIGHT-WATER-REACTOR SAFETY
FUEL SYSTEMS RESEARCH PROGRAMS
QUARTERLY PROGRESS REPORT

April-June 1984

ABSTRACT

This progress report summarizes work performed by the Materials Science and Technology Division of Argonne National Laboratory during April, May, and June 1984 on water reactor safety problems related to fuel and cladding. The research and development areas covered are Transient Fuel Response and Fission Product Release and Clad Properties for Code Verification.

NRC Fin No.	FIN Title
A2016	Transient Fuel Response and Fission Product Release
A2017	Clad Properties for Code Verification

TABLE OF CONTENTS

LIGHT-WATER-REACTOR SAFETY
FUEL SYSTEMS RESEARCH PROGRAMS:
QUARTERLY PROGRESS REPORT

April-June 1984

EXECUTIVE SUMMARY

I. TRANSIENT FUEL RESPONSE AND FISSION PRODUCT RELEASE[a]

A tellurium release model, which is based upon thermochemical considerations and a synthesis of available data, has been incorporated into the FASTGRASS-VFP code. This model treats Te behavior in the fuel as well as Te sequestering by Zircaloy cladding. The model for Te behavior in the fuel includes the effects of Te generation, decay, solubility, diffusivity, and interaction with intra- and intergranular microbubbles. The models for Te tie-up by Zircaloy and subsequent release upon Zr cladding oxidation are similar to the quantitative Te release criteria recently suggested by Lorenz et al.

FASTGRASS-VFP-calculated Te release has been validated against SFD-ST data.

---

[a]RSR FIN Budget No. A2016; RSR Contact: L. Chan.

II. CLAD PROPERTIES FOR CODE VERIFICATION[b]

Zircaloy fuel cladding is susceptible to local breach-type failures during power transients in LWRs because of stresses imposed by differential thermal expansion of the fuel and cladding. In this program, the effect of stress state, strain rate, and temperature on the deformation characteristics of irradiated Zircaloy fuel cladding is being investigated to provide mechanical-property information and a failure criterion for the cladding under loading conditions conducive to pellet-cladding interaction (PCI). The information will be used in the development of codes to analyze PCI in fuel rods from power ramp experiments in test reactors, and to evaluate the susceptibility of extended-burnup fuel elements and new fuel element designs in commercial reactors to PCI failures during power transients.

Pellet-cladding interaction in-reactor is usually characterized by a highly localized stress and a mechanical constraint in the cladding produced as a result of the friction between the expanding pellet and cladding inner surface. The mechanical constraint is conducive to a plane-strain deformation condition of the highly anisotropic cladding. Under such a condition, the local cladding material is more susceptible to a low-ductility PCI failure. In this reporting period, the existing expanding-mandrel apparatus was modified to incorporate an axial mechanical constraint. A deformation test on H. B. Robinson spent-fuel cladding with the modified expanding-mandrel apparatus successfully simulated a PCI failure. Evidence was obtained for propagation of a brittle crack at room temperature in a piece of cladding that contained incipient PCI-like cracks. The instantaneous propagation of the crack is inconsistent with a stress-corrosion cracking model but indicates a general embrittlement of the particular cladding specimen.

From TEM examination of thin-foil specimens obtained from ductile-failure tubes (i.e., tubes with no or a negligible amount of pseudocleavage on the fracture surface), numerous dislocations with $\frac{1}{3}\langle 11\bar{2}0\rangle$ Burgers vectors and slip traces were observed. In contrast, the specimens that failed in a brittle manner with a large extent of pseudocleavage did not show indications

[b]RSR FIN Budget No. A2017; RSR Contact: H. H. Scott.

of appreciable dislocation activity. Compared to the ductile-failure specimens, only a limited number of entangled dislocations were observed in the brittle-failure specimens. The dislocation entanglements were invariably observed in association with clusters of precipitates and/or irradiation-induced defects. In dark-field contrast, individual dislocations decorated by precipitates smaller than 10 nm in size could be observed. In addition, superlattice reflections corresponding to ordered oxygen in the Zr_3O structure could be observed in the selected-area diffraction patterns obtained from the dislocation-entanglement/cluster complexes, indicating an irradiation-enhanced segregation of oxygen to the dislocation substructure. Diffraction characteristics of a large number of dislocation entanglements in both ductile- and brittle-failure specimens were analyzed. Zr_3O superlattice reflections were observed in ~61% of the analyzed diffraction patterns for brittle-failure specimens, compared to ~9% in the case of ductile-failure specimens.

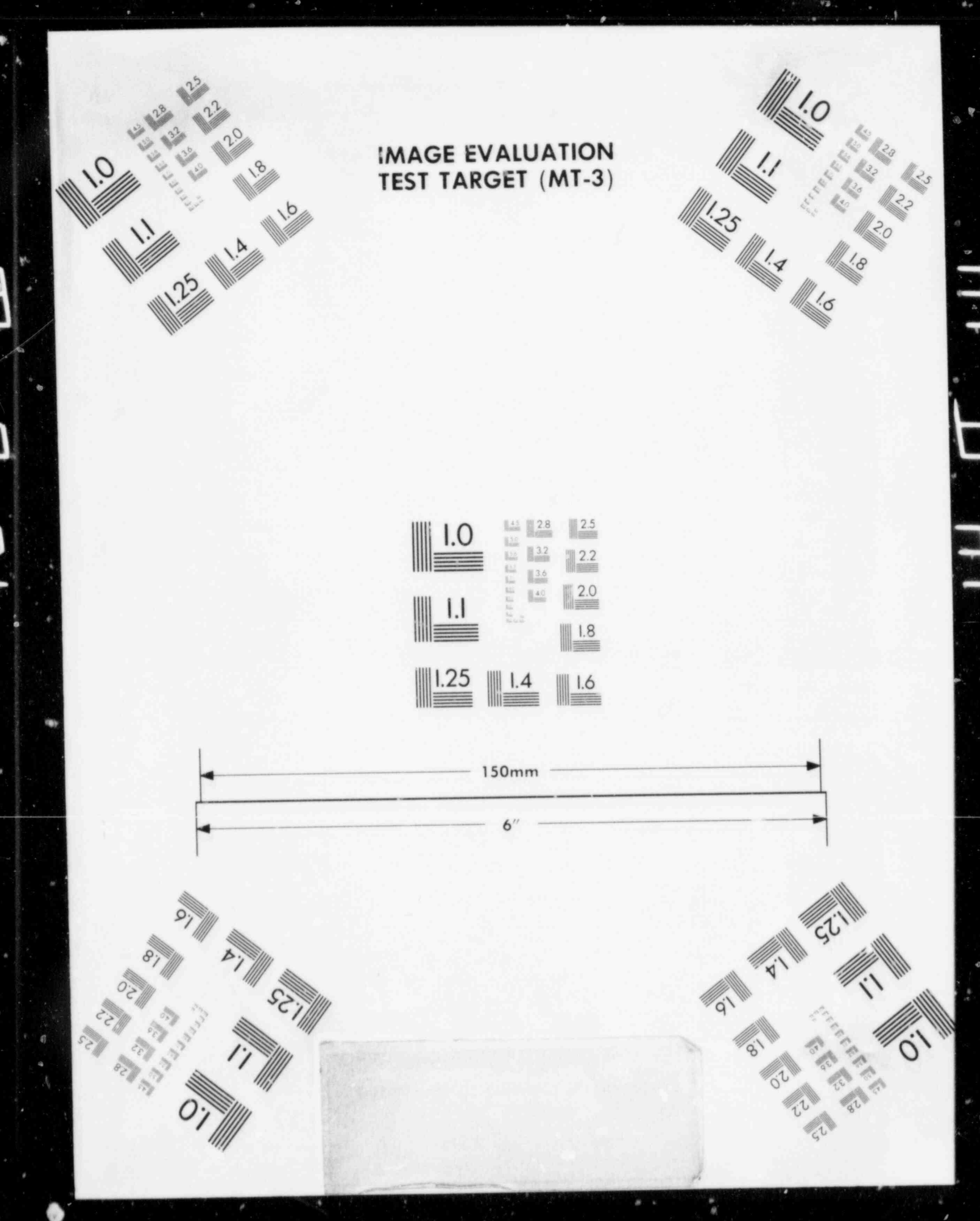
IMAGE EVALUATION
TEST TARGET (MT-3)
1.0
1.1
1.25
1.4
1.6
1.8
2.0
2.2
2.5
2.8
3.2
3.6
4.0
150mm
6"

IMAGE EVALUATION
TEST TARGET (MT-3)

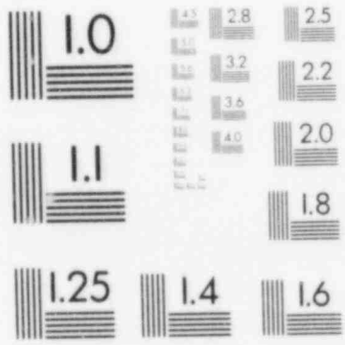

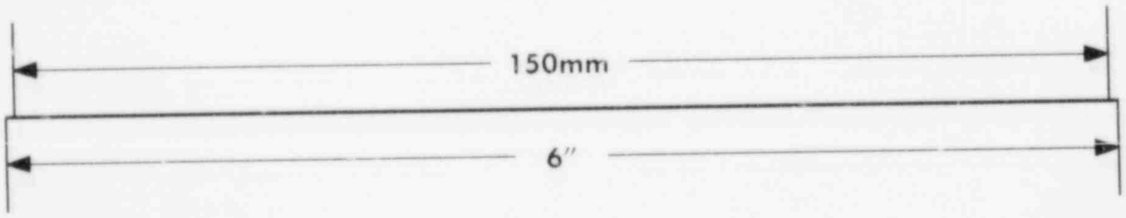

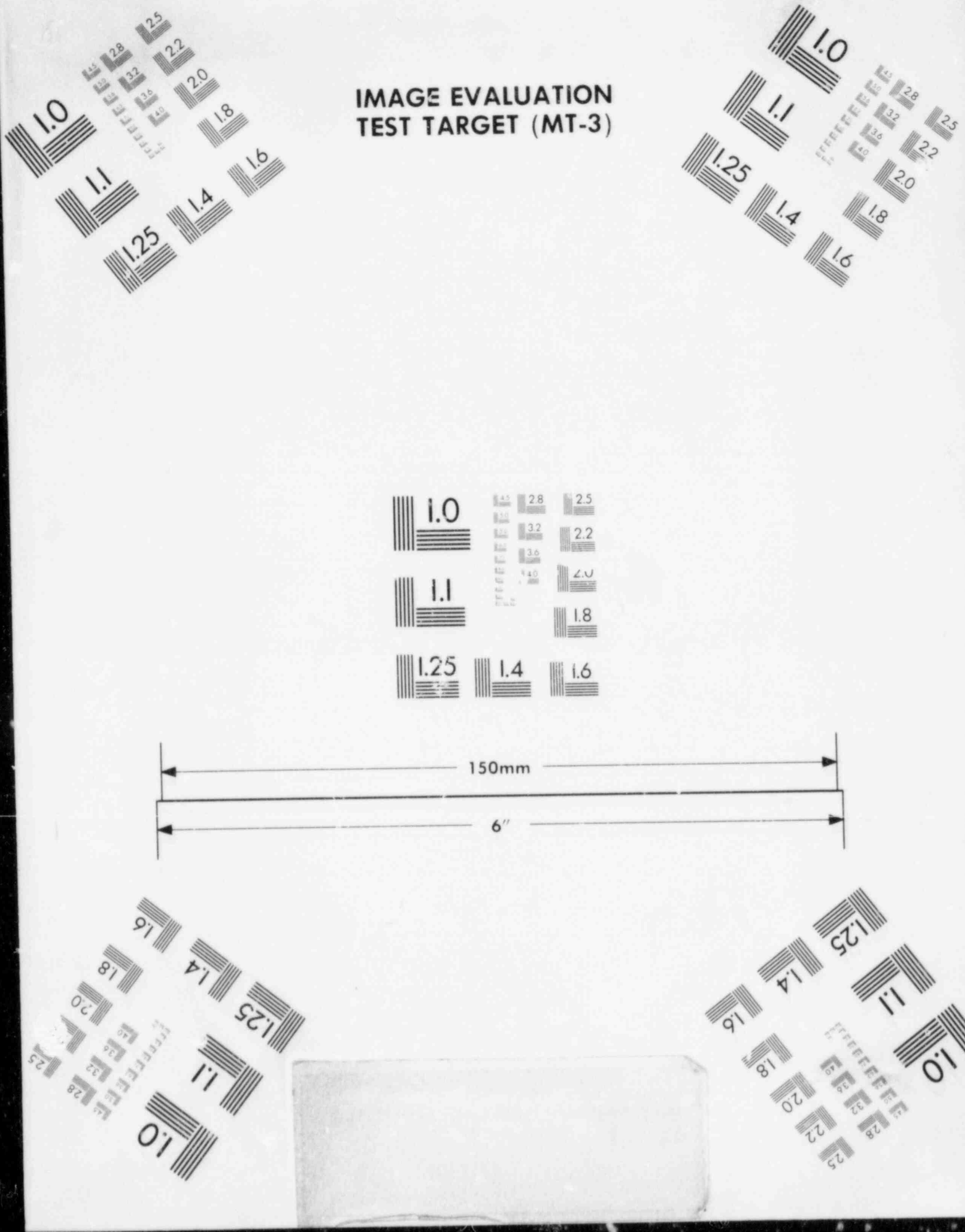
IMAGE EVALUATION
TEST TARGET (MT-3)
1.0
1.1
1.25
1.4
1.6
1.8
2.0
2.2
2.5
2.8
3.2
3.6
4.0
150mm
6"

I. TRANSIENT FUEL RESPONSE AND FISSION PRODUCT RELEASE

Principal Investigator:
J. Rest

A. FASTGRASS-VFP Model Development to Include Tellurium Release from Severely Damaged UO_2 Fuel (J. Rest and A. W. Cronenberg*)

FASTGRASS-VFP[1-3] is a mechanistic computer model for predicting the distribution and release of fission gas and volatile fission products (VFPs) in solid UO_2-based fuels during steady-state and transient conditions. Models are included for the calculation of fission product generation; gas bubble nucleation and re-solution; bubble migration and coalescence; interaction between I, Cs, CsI, and fission gas bubbles; chemical reaction between Cs and fuel; channel formation on grain faces; interlinked porosity on grain edges; and microcracking. Fission products released from the fuel are assumed to reach the pellet surface by successively migrating from the grain interior to grain faces and then to the grain edges, with subsequent transport through a network of interconnected tunnels and as-fabricated porosity. The present version of the code models the fission gases Xe and Kr; the volatiles I and Cs; and the major VFP reaction products, CsI, Cs_2MoO_4, and Cs_2UO_4. Recently a model has been incorporated into FASTGRASS to account for tellurium (Te) release.

As indicated in Table 1.1, iodine is the primary risk-dominant radionuclide affecting the health consequences associated with fission product release for severe-core-damage LWR accidents. The next most important species is tellurium (Te), followed by cesium (Cs). As discussed by Lorenz,[4,5] although the risk associated with Te is only slightly lower than that of iodine, its release and transport in source-term experiments is often overlooked. This is because in spent test fuel (fuel which has been out of the reactor for a period of time), only stable Te isotopes (^{128}Te and ^{130}Te) are present, all short-lived isotopes having decayed to other

---

*Consultant, Engineering Science and Analysis, 836 Claire View, Idaho Falls, Idaho 83402.

elements via beta-emission. Therefore, Te discharge from such fuel cannot be detected by on-line real-time gamma counting. In addition, the fission yield of stable Te isotopes exhibits a proportionate ratio similar to what is found in nature. In a posttest examination, it is thus difficult to distinguish Te fission product deposits from naturally occurring Te. Because of such difficulties, Te release has not been studied or qualified to the extent that the noble gases (Xe, Kr) and volatiles I and Cs have. Nevertheless, because of its importance, an understanding of Te release behavior is essential for qualification of severe-accident source-term models.

Table 1.1
Importance Ranking of Radionuclides with Respect to Health Effects

Element	Rank	Ranking Factor
Iodine, I	1	38
Tellurium, Te	2	37
Cesium, Cs	3	31
Strontium, Sr	4	16
Ruthenium, Ru	5	15
Barium, Ba	6	11

A Te release model for FASTGRASS-VFP and a comparison of calculated results with recent SFD-ST data are described in this report. First, however, a brief review is presented on the physical and chemical properties affecting Te escape from Zircaloy-clad UO_2 fuel, and the data base used in support of model development.

1. Te Physical/Chemical Properties Affecting Release

Tellurium is one of the Group-VI elements, on the far right of the periodic table, of which oxygen is the most abundant. These elements have relatively high ionization potentials, and metallic properties are hard to find. However, electrons are held less tightly for the heavier elements, and hence there is some suggestion of metallic behavior for Te. As discussed by Blackburn and Johnson,[6] the thermochemical data available to develop a predictive capability for Te release from fuel are quite limited.

Basically, the available thermochemical data on Te are those given in the JANAF tables and by Barin et al.[7] Blackburn and Johnson used such data to derive linear equations for the free energy of formation (ΔG_f) of the tellurides formed with various fission products, as well as with hydrogen, oxygen, iron, and nickel. Their estimates of ΔG_f indicated that the lanthanide and alkaline-earth tellurides would be stable. However, the lanthanides and alkaline earths, as well as Zr, Ba, Sr, and Mo, form more stable oxides in UO_2 and thus would not be expected to form tellurides in irradiated fuel. Of the remaining tellurides, only fission product Cs is of high enough concentration that it might be expected to form a stable telluride within UO_2. Although the compound Cs_2Te is mentioned in the literature,[8] thermochemical data for this compound have not been established. Blackburn and O'Hare[9] were not able to prepare this compound from cesium and tellurium in a ratio of 2:1.

The free energy of formation of tellurium oxide is higher than that of UO_2, indicating that Te should reside in the metallic rather than the oxide state. In sum, equilibrium data, albeit quite limited, indicate that the sequestering potential of Te by the majority of fission products or free oxygen in UO_2 is unlikely; thus, the release of Te is considered essentially governed by its atomic diffusivity in UO_2. However, in the presence of Zircaloy cladding, sequestering may occur.

Tellurium (atomic weight = 127.6) reacts readily with Zr (atomic weight = 91.2) to form at least six known stable compounds, collectively known as the zirconium tellurides:[10]

Zirconium monotelluride, ZrTe (58.32 wt-percent Te),
Zirconium ditelluride, $ZrTe_2$ (73.67 wt-percent Te),
Zirconium tritelluride, $ZrTe_3$ (80.76 wt-percent Te),
Zirconium sesquitelluride, Zr_2Te_3 (67.73 wt-percent Te),
Trizirconium ditelluride, Zr_3Te_2 (48.27 wt-percent Te),
Tetrazirconium tritelluride, Zr_4Te_3 (51.20 wt-percent Te).

No thermodynamic data are given in the JANAF tables for the various zirconium tellurides, nor are their thermophysical properties well

known. However, estimated free energies of formation (ΔG_f) for $ZrTe_2$ and $ZrTe_3$ have been presented by Mills:[11]

For Zr (solid) + Te_2 (gas) = $ZrTe_2$ (solid),

$$\Delta G_f = -107500 + 40.13\ T \quad (298\ K \leq T \leq 1870\ K);$$

for Zr (solid) + 3Te (liquid) = $ZrTe_3$ (solid),

$$\Delta G_f = -86.800 + 40.59\ T \quad (723 \leq T \leq MP).$$

As discussed by Lorenz et al.,[4,5] the reaction of Te with zirconium and the desorption of tellurium may be sensitive to oxidation effects. The free energies of formation of ZrO_2 and TeO_2 at 1500 K are -195 and -12 kcal/mol O_2, respectively, thus indicating the higher stability of ZrO_2. Such thermodynamic considerations indicate that if the Zircaloy cladding is completely oxidized, little sequestering of Te by the oxidized cladding should occur. This effect was observed in several ORNL experiments reviewed below.

2. Effects of Zirconium Cladding on Te Release

In various ORNL experiments, the release rates of Te from unclad UO_2 have generally been high, that is, within a factor of 2 of iodine. When tests were conducted with Zircaloy cladding, however, significantly lower release rates were noted if the cladding was not fully oxidized. Table 1.2 shows Te release data from early studies conducted by Parker,[12] in which bare UO_2 samples were heated in an inert or reducing environment. The release of Te is shown to be similar in magnitude to that of iodine.

More recent out-of-reactor fission product release and aerosol generation tests[13] have also been conducted at ORNL, with Zircaloy-clad 8-in.-long samples of previously irradiated fuel. In this test series, fuel is induction heated in a flowing steam environment under conditions that simulate a relatively slow decay-heat/loss-of-coolant accident. Tellurium

Table 1.2
Results of Release Tests with Unclad UO_2 Samples

Experiment Description	Burnup (MWd/MT)	Temperature (C)	Time (min)	Percent Released			
				Xe,Kr	I	Te	Cs
Diffusion	1	1200	330	0.3	0.57	0.63	0.11
		1600	330	2.3	6.0	12.0	1.5
		2000	330	19.0	40.0	65.0	16.0
Diffusion	4000	1200	330	1.4	6.5	6.5	6.5
		1600	330	13.0	40.0	40.0	40.0
		2000	330	80.0	84.0	84.0	84.0
Tungsten crucible	1	2800	2	99.0	94.0	97.0	69.0

deposits on the test apparatus are measured by Spark Source Mass Spectrometry (SSMS). Data for the test runs conducted to date are listed in Table 1.3.

Table 1.3
Te Release Behavior Noted in the ORNL-HI Test Series

Test No.	Temperature (C)	Time (min)	I, Cs, Kr Release (percent)	Te Release (percent)	Zircaloy Oxidized (percent)
HI-1	1400	30	2	0.3	40
HI-2	1700	20	50	50-100	100
HI-3	2000	20	55	0.6	35

Although the tellurium release amounts are only approximate, it is clear that much more tellurium was released in Test HI-2 than in the other tests. The extent of oxidation of the Zircaloy was essentially complete in test HI-2. The low oxidation fraction shown for Tests HI-1 and HI-3 is a result of the limited steam supply and the relocation of the Zircaloy after melting. After synthesizing of these and other data, Lorenz et al.[4,5] summarized Te release behavior for Zircaloy-clad fuel rods as follows:

> The rate of escape of tellurium from the UO_2 fuel itself is considered approximately equal to that of iodine, over the temperature range 1200 to 2800°C. However, when unoxidized Zircaloy cladding is present, the Zircaloy retains the tellurium and the release from the fuel rod is drastically reduced, typically by a factor of 30. However, if Zircaloy oxidation is complete or nearly so, Te sequestering by Zr is reduced and release is controlled by the fuel only.

Such behavior is supported by the Te release behavior noted in recent PBF-SFD tests.

Figure 1.1 presents a comparison of the measured Te behavior for the SFD-ST and 1-1 tests.[14,15] (Also shown in Fig. 1.1 are the FASTGRASS-VFP calculated values for the Te fractional release rate for the SFD-ST test. These calculated results will be discussed in a later section.) As indicated, Te reached the fission product detection system and was measured during the high-temperature ($T \leq 1800$ K) heatup phase of the scoping test. By contrast, however, little Te was detected during either the heatup or

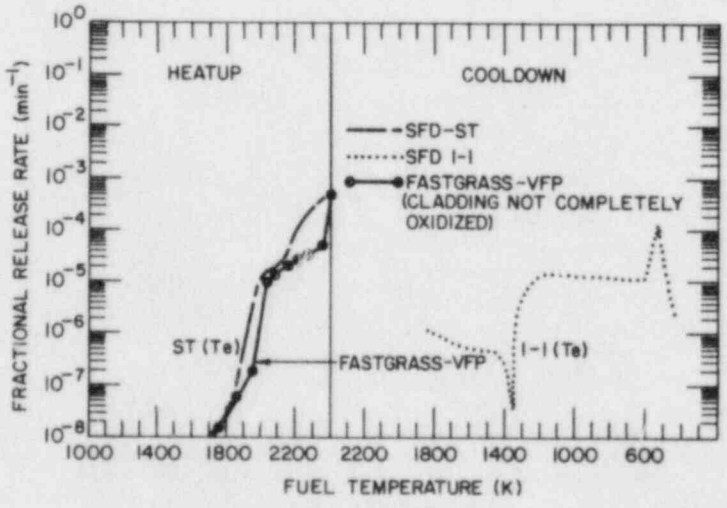

Fig. 1.1
Comparison of the SFD-ST and 1-1 Te Release Data.

cooldown phase of the SFD 1-1 test. Such differences in measured Te behavior may be explainable, in part, in terms of Te-cladding interactions.

With respect to Te-Zr reaction chemistry, the scoping test was essentially steam-rich, such that significant Zircaloy cladding oxidation is anticipated. Indeed, the on-line real-time measurement of H_2 release during the test indicates that at the time of significant fission product release the Zircaloy cladding would have been completely oxidized in the major portion of the ST-bundle. Since the free energy of formation of TeO_2 (-12 kcal/mole) is less negative than that of ZrO_2 (-195 kcal/mole), ZrO_2 is stable in the presence of Te; thus, little sequestering of Te by ZrO_2 would be expected. This thesis is supported by the observed release of Te measured in the SFD-ST experiment. For the steam-starved conditions of the SFD 1-1 test, however, the hydrogen release data indicate a maximum of 30 percent cladding oxidation; thus, significant sequestering of Te by unoxidized Zr would be anticipated, via the reaction

$$Zr(s) + 2Te(g) = ZrTe_2(s).$$

The fact that little initial Te release was detected during the 1-1 test might be indicative of its sequestering by unoxidized Zr. However, the analysis of the data is in the initial stage, and a definitive conclusion about the behavior of Te is not yet possible.

On the basis of thermochemical considerations and a synthesis of the ORNL and SFD-ST data, the following Te release model was incorporated into the FASTGRASS-VFP code. Such a model is similar to the quantitative Te release criteria recently suggested by Lorenz et al.[4,5]

3. FASTGRASS-VFP Te Release Model

Since Te release from bare UO_2 samples, as well as diffusion data,[16] indicates similar Te and I mobilities, the overall transport processes within the fuel matrix for Te are assumed to mirror that of I. However, unlike iodine, for which FASTGRASS-VFP calculates CsI formation,

all fission-product tellurium is assumed to remain in an unbound chemical state. The necessary parameters and scaling factors used in the calculation of Te release, based on the FASTGRASS-predicted I release behavior,[1-3] are as follows:

Effective Te Generation Rate: On the basis of decay chain calculations, the effective Te generation rate at chemical equilibrium is 0.0252 Te atoms/fission.

This value is a code input parameter, which can be user-specified for irradiation conditions where chemical equilibrium has not been attained.

Solubility Coefficient: equivalent to that of iodine, based on similarity of valence (i.e., Te^{-2}, I^{-1}) and atomic radius (i.e., Te = 1.37Å, I = 1.33Å).

Atomic Diffusivity in UO_2: the same as iodine, based on the findings of Turnbull and Friskney,[16] i.e.,

$$D_{Te} = D_I = 2.1 \times 10^{-4} \exp[-91{,}000/(1.987T)], \text{ cm}^2/\text{s},$$

where T = temperature (K).

Intragranular Microbubble Diffusivity: taken to have the same capture probability within intragranular microbubbles as iodine. Diffusivity of microbubbles assumed unaltered by presence of Te, I, or Cs.

Intergranular Macrobubble Behavior: As with the case of I and Cs, all Te swept to grain boundaries is assumed to be captured by gaseous intergranular macrobubbles, where the release of such fission product is controlled by the interlinked porosity criterion presently employed in FASTGRASS-VFP.

Te Sequestering by Zircaloy Cladding: Tie-up of Te by Zircaloy is based upon the cladding oxidation criteria suggested by Lorenz et al.[4] When the local degree of cladding oxidation (i.e., in a control volume or node) is estimated to be less than 90 percent, the tellurium release rate from the rod (fuel plus cladding) is reduced by a factor of 1/40th the calculated Te release rate from the fuel microstructure. This criterion assumes 97.5 percent (39/40) of Te released from fuel microstructure is sequestered by the cladding. When the local degree of cladding oxidation is predicted to reach or exceed 90 percent, no reduction in release rate is assumed to occur.

Cladding Oxidation: Since the present version of the FASTGRASS-VFP code does not include models for the prediction of cladding behavior, cladding oxidation state is user specified. An axial cladding node is specified for each fuel node, where the user can define a time-independent or time-dependent cladding oxidation state.

Calculational results and comparison with the recent SFD-ST Te release data are presented below.

4. Calculational Results

In addition to the data, Fig. 1.1 gives the FASTGRASS-VFP-calculated values for the Te fractional release rate as a function of the maximum fuel temperature for the SFD-ST test. For these calculations, it was assumed that the SFD-ST cladding was not completely oxidized during the period over which the calculations were made (i.e., during the initial phase of the accident up to a peak temperature of 2400 K). This assumption is consistent with the total hydrogen release data for the SFD-ST test, which indicates that at the time the fuel temperatures reached 2400 K (~202.5 minutes into the transient), the cladding was not yet completely oxidized.

Although this initial comparison between FASTGRASS-VFP predicted Te release and the measured data is reasonable, the analysis is incomplete in the sense that models are lacking for the timed release of Te from completely oxidized Zircaloy cladding. In addition, a better understanding of the behavior of the volatile fission products during transport through the effluent line to the detectors is required in order to better understand fission product release from the fuel rod. For example, to what degree are the different steam flow rates between the SFD-ST and the SFD 1-1 test reflected in the differences in the Te release rates shown in Fig. 1.1? These questions are currently being addressed. The results of these efforts will be reported in the future.

B. References for Chapter I

1. J. Rest, "Volatile Fission-Product Source Term Evaluation Using the FASTGRASS Computer Code," in Proc. Intern. Mtg. Thermal Reactor Safety, Chicago, IL, August 29-September 2, 1982, pp. 111-121.

2. J. Rest, Evaluation of Volatile and Gaseous Fission Product Behavior in Water Reactor Fuel Under Normal and Severe Core Accident Conditions, Nucl. Technol. 61, 33-48 (1983).

3. J. Rest, "The Mechanistic Prediction of Xenon, Iodine, and Cesium Release from LWR Fuel Under Degraded-Core Accident Conditions,"to be published in Proc. ANS Topical Meeting on Fission Product Behavior and Source Term Research, Snowbird, Utah, July 15-19, 1984.

4. R. A. Lorenz, E. C. Beahm, and R. P. Wichner, Review of Tellurium Release Rates from LWR Fuel Elements and Aerosol Formation from Silver Control Rod Materials, ORNL Report, to be published, 1984.

5. R. A. Lorenz, E. C. Beahm, and R. P. Wichner, "Review of Tellurium Release Rates from Fuel Elements Under Accident Conditions," to be published in Proc. International Meeting on Light Water Reactor Severe Accident Evaluation, Cambridge, MA, August 28-Sept. 1, 1983.

6. P. E. Blackburn and C. E. Johnson, Light Water Reactor Fission Product Data Assessment, ANL-82-42 (Sept. 1982).

7. I. Barin, O. Knacke, and O. Kubaschewski, Supplement Thermochemical Properties of Inorganic Substances, Springer Verlag, Berlin (1977).

8. W. Klemn, H. Sodomann, and P. Langmesser, Z. Anorg. Allg. Chem. 241, 281 (1939).

9. P. E. Blackburn and P. A. O'Hare (ANL), personal communication, May 16, 1984; no thermochemical data was obtained for the Cs-Te system.

10. D. M. Chizhikov and V. P. Shchastlivyi, Tellurium and the Tellurides, Collet's Pub. Co., London (1970).

11. K. C. Mills, Thermodynamic Data for Inorganic Sulfides, Selenides, and Tellurides, Butterworths, London (1974).

12. G. W. Parker et al., Out-of-Pile Studies of Fission-Product Release from Overheated Reactor Fuels at ORNL: 1955-1965, ORNL-3981 (1967).

13. M. F. Osborne, R. A. Lorenz, J. R. Travis, and C. S. Webster, Data Summary Report for Fission Product Release: Test HI-1, NUREG/CR-2928, ORNL/TM-8500 (December 1982).

14. D. J. Osetek, A. W. Cronenberg, R. R. Hobbins, and K. Vinjamuri, "Fission Product Behavior During the First Two PBF Severe Fuel Damage Tests," to be published in Proc. ANS Topical Meeting on Fission Product Behavior and Source Term Research, Snowbird, Utah, July 15-19, 1984.

15. A. W. Cronenberg et al., "An Assessment of Liquefaction-Induced I, Cs, and Te Release from Low and High Burnup Fuel," to be published in Proc. International Meeting on Light Water Reactor Severe Accident Evaluation, Cambridge, MA, August 28-September 1, 1983.

16. J. A. Turnbull and C. A. Friskney, The Release of Fission Products from Nuclear Fuel During Irradiation by Both Lattice and Grain-Boundary Diffusion, J. Nucl. Mater. 58, 31-38 (1975).

II. CLAD PROPERTIES FOR CODE VERIFICATION

Principal Investigators:
H. M. Chung, F. L. Yaggee, and T. F. Kassner

The Zircaloy cladding of fuel rods in light-water-cooled reactors is susceptible to local breach-type failures, commonly known as pellet-cladding interaction (PCI) failures, during power transients after the fuel has achieved sufficiently high burnup. As a result of the high burnup, the gap between the UO_2 fuel pellets and the cladding is closed and highly localized stress is believed to be imposed on the cladding by differential thermal expansion of the cracked fuel and cladding during power transients. In addition to the localized stress, a high-burnup fuel cladding is also characterized by high-density radiation-induced defects (RID), mechanical constraints imposed by pellet-cladding friction, compositional changes (e.g., oxygen and hydrogen uptake associated with in-service corrosion), and geometrical changes due to creep-down and bowing. It is possible that synergistic effects involving more than one of the above factors influence the deformation and fracture of the in-reactor fuel cladding, e.g., strain aging associated with impurity or alloying elements, irradiation- or stress-induced segregation of the elements and subsequent formation of non-equilibrium phases. Although mechanisms of stress corrosion cracking (SCC) associated with volatile fission products such as I and liquid metal embrittlement (LME) associated with an element such as Cd have been well established for local breach-type failures of irradiated and unirradiated Zircaloy cladding under out-of-reactor simulation conditions, conclusive evidence of these processes is not yet available for in-reactor PCI failures. Consequently, to provide a better understanding of the PCI phenomenon, we have undertaken a mechanistic study of the deformation and fracture behavior of actual power-reactor fuel cladding discharged after a high burnup.

In this program, the effect of temperature, strain rate, and stress localization on the deformation and fracture characteristics of Zircaloy cladding from spent-fuel rods is being investigated by means of internal gas-pressurization and mandrel-loading experiments in the absence of simulated fission product species. The deformed and fractured specimens of spent-fuel

cladding are then being examined by optical microscopy, scanning electron microscopy (SEM), transmission electron microscopy (TEM), and high-voltage electron microscopy (HVEM). The results of microstructural and fracture-property investigations will be used to develop a failure criterion for the cladding under PCI-type loading conditions. The information will be incorporated into fuel performance codes, which can be used to evaluate the susceptibility of extended-burnup fuel elements in commercial reactors to PCI failures during power transients in later cycles, and to evaluate cladding performance and reliability of new fuel-element designs. An optimization of power ramp procedures to minimize cladding failures would result in a significant decrease in radiation exposure of plant personnel due to background and airborne radioactivity as well as an extension of core life in terms of allowable off-gas radioactivity.

A. Fracture Characteristics of H. B. Robinson Cladding by Modified Expanding-Mandrel Loading (H. M. Chung)

1. Introduction

Design and fabrication of the fixture that was used to provide axial constraint during cladding deformation by an expanding-mandrel technique have been reported elsewhere.[1] The fixture was assembled and tested using unirradiated Zircaloy outside of the hot cell. After several successful tests, the in-cell expanding mandrel apparatus was modified to incorporate the fixture and was used to fracture several H. B. Robinson spent-fuel cladding tubes at 325°C. Because of the constraining fixture, specimen tube deformation in the axial direction was minimal. This, in turn, produces a higher axial-to-tangential stress ratio in the local region that is loaded by the expanding ring. In this manner, the stress state in the local expanding region (i.e., the "ridge") is expected to be similar to that of an in-reactor PCI situation, although the deformation condition may not be rigorously plane-strain.

2. Brittle-type Failure

H. B. Robinson cladding specimen 217A4G was tested in the modified expanding-mandrel apparatus at 325°C in a manner similar to those of specimens

217A4C, E, and F of Table 3.1, Ref. 2. Visible cracks on the outer surface similar to those of Figs. 3.24 and 3.28 of Ref. 3 could not be identified unambiguously in the ridged region. The ridged region was cut into two clamshells in a manner outlined in Fig. 51 of Ref. 4. Outer surfaces of both clamshells were examined by SEM to determine the location of a through-wall crack. SEM examination could not identify the outer-surface failure site. However, numerous incipient cracks were observed on the inner surface of the clamshells as shown in Fig. 2.1. The incipient cracks visible in Fig. 2.1 are clearly associated with the location of the expanding ring (i.e., along the stress-concentrated circumference). This indicates that the incipient cracks were produced during the expanding-mandrel test under an inert gas environment but not during in-reactor service.

To open and reveal the fracture surfaces of the incipient crack, which is denoted by the circle in Fig. 2.1(A), two notches were going to be made at the arrowed positions in alignment with the incipient crack. The first (notch S) was made at room temperature in the glovebox with wire-cutting pliers. However, the notch crack propagated instantaneously along the whole length of ~10 mm of the clamshell. The room-temperature crack propagated right through the incipient crack as shown in the circle of Fig. 2.1(B). The overall view of the fracture surface is shown in Fig. 2.2(A), with some selected areas (circled) magnified in Figs. 2.2(B), (C), and (D).

The fracture surface morphology shown in Fig. 2.2 clearly indicates a large extent of pseudocleavage that is characteristic of a PCI failure. The figure also reveals steps invariably perpendicular to the radial-tangential plane of the cladding tube. The morphology of the step surface is always ductile dimple. A similar fracture surface morphology has been reported for in-reactor PCI failures.[5,6]

The brittle crack propagation observed at room temperature during notching of the specimen, as described above, also occurred for the other matching clamshell. This clearly indicates a general embrittlement of the specimen piece. It is not clear, however, whether the embrittlement was primarily as a result of the in-reactor service or a result of the out-of-reactor expanding-mandrel loading. In either case, the fact that the brittle

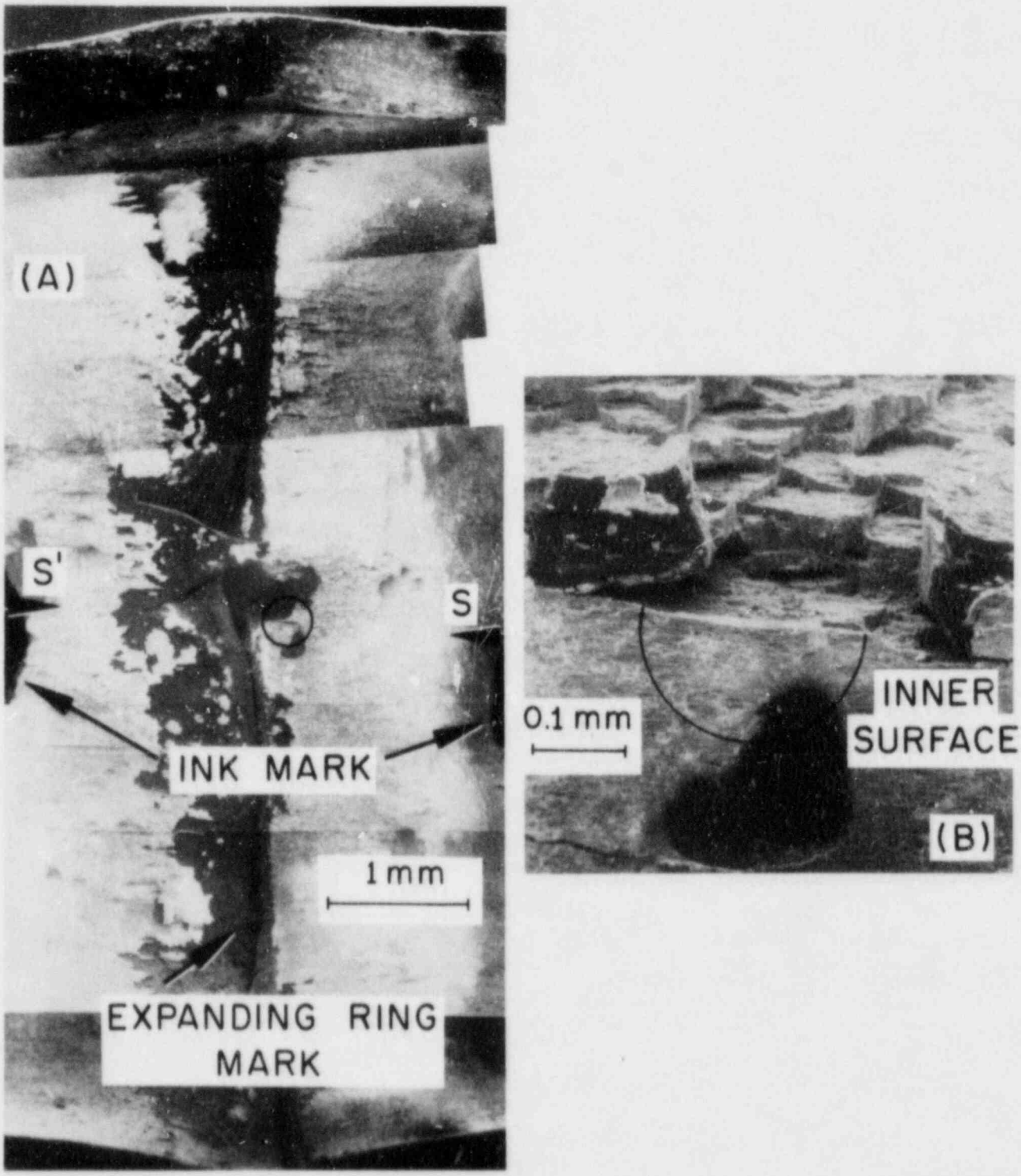

Fig. 2.1. Morphology of Incipient Cracks on the Inner Surface of an H. B. Robinson Cladding Specimen 217A4G Produced during Expanding Mandrel Test at 325°C. (A) Overall view showing cracks along the compression mark of the expanding ring; (B) higher magnification of the circled crack in (A) after room-temperature fracture along the line connecting the arrows. The room-temperature fracture propagated instantaneously in brittle manner from arrow S through the encircled incipient crack.

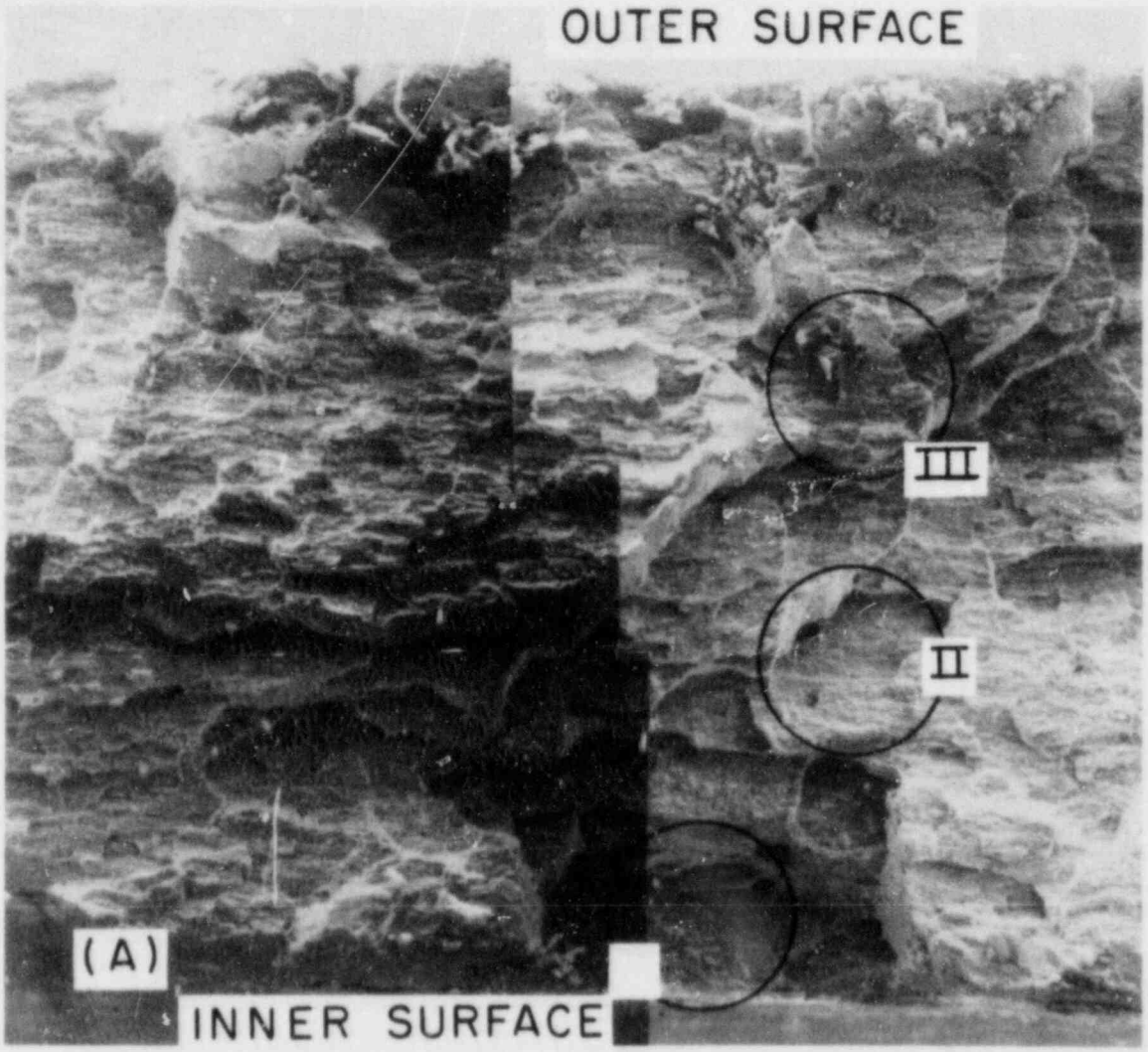

Fig. 2.2. Fracture Surface Morphology Near the Crack Shown in Fig. 2.1(B). (A) Overall view of the fracture surface; (B), (C), and (D) higher magnifications of circled areas I, II, and III, respectively, of (A) showing pseudocleavage.

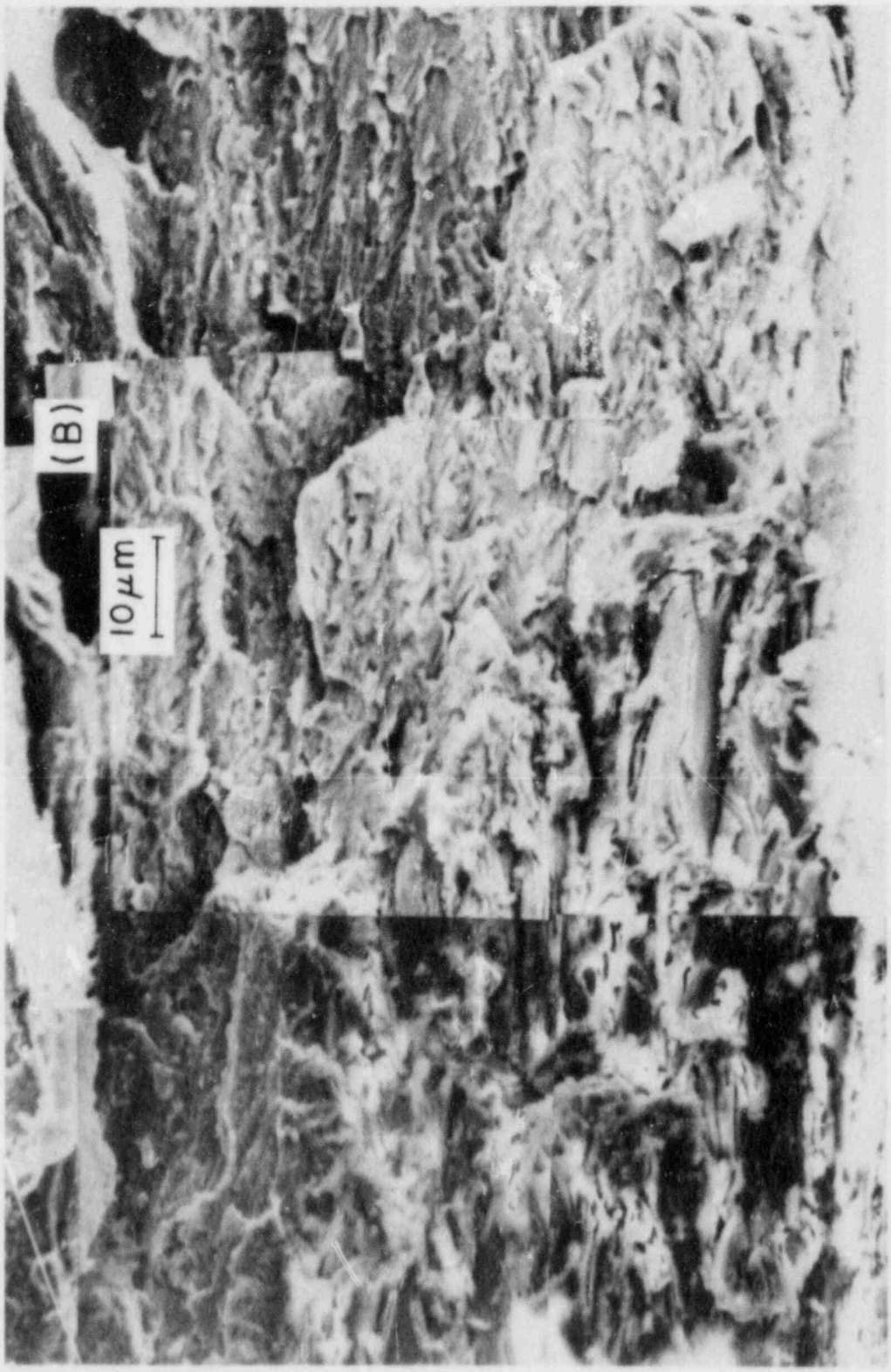

Fig. 2.2. (Contd.)

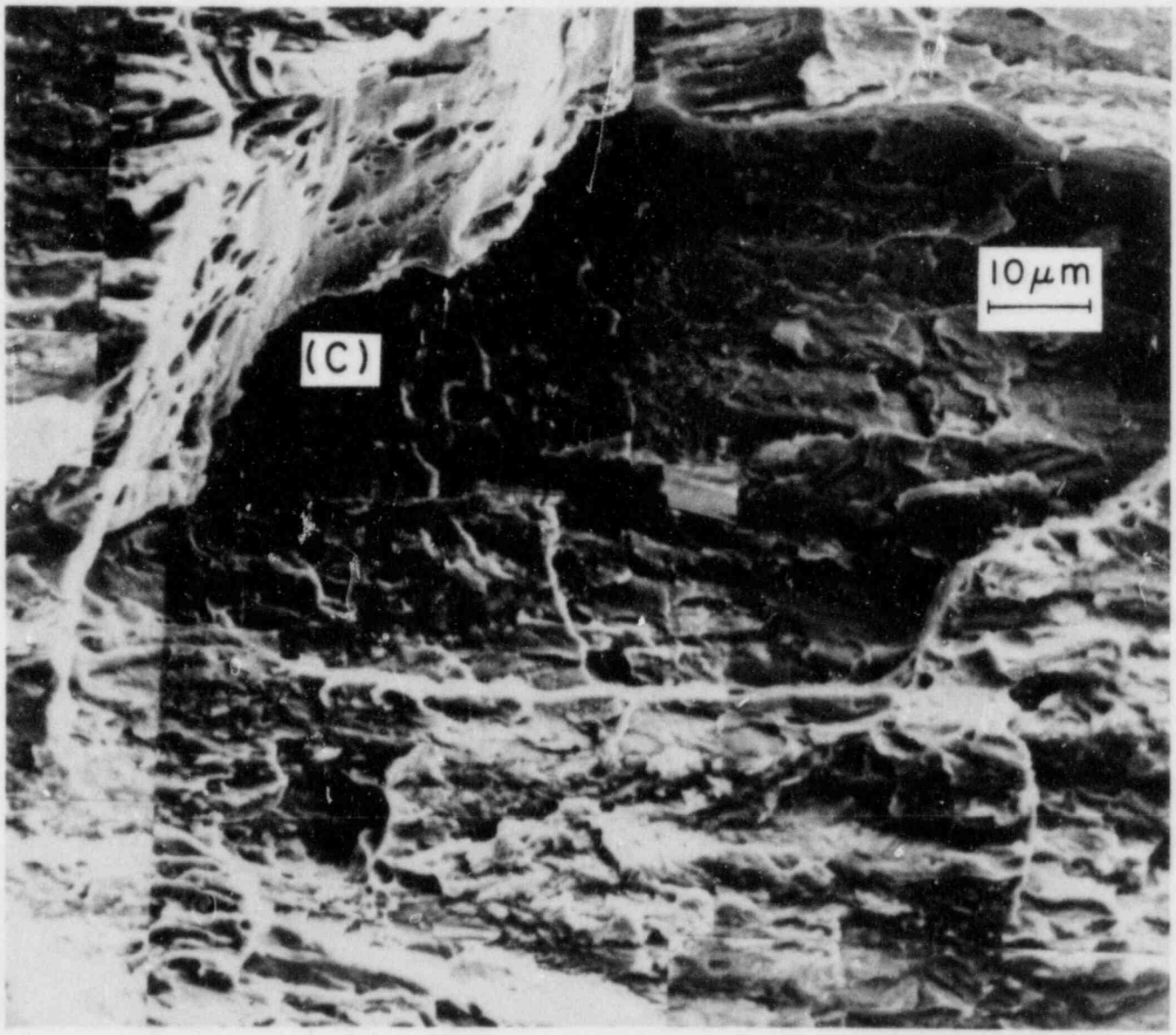

Fig. 2.2. (Contd.)

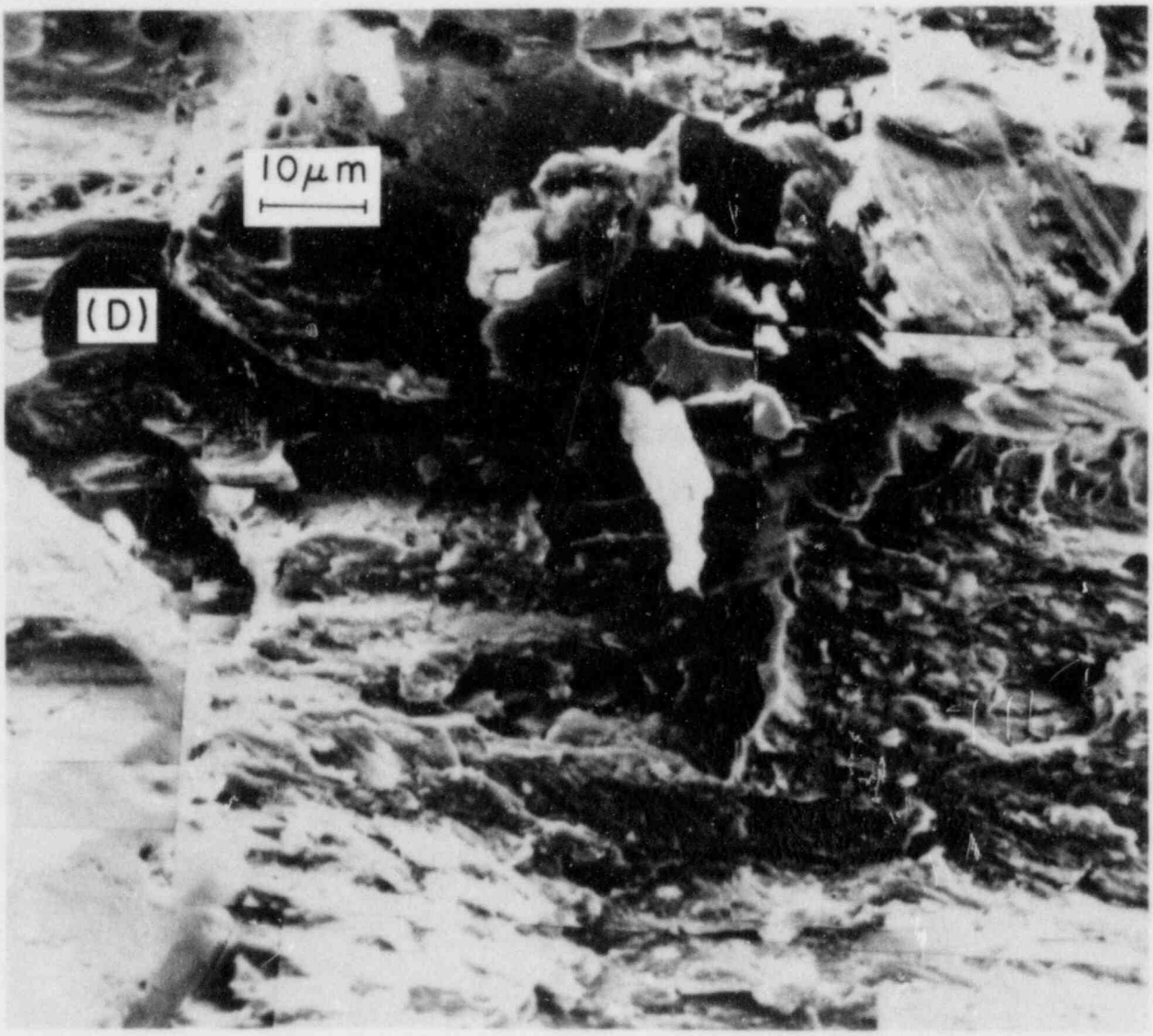

Fig. 2.2. (Contd.)

crack propagated instantaneously is not consistent with a stress-corrosion cracking process, simply because there would be no time for transport of a corrosion agent in the material. Brittle-type failures under fast loading conditions that are incompatible with stress-corrosion cracking have been reported elsewhere for irradiated Zircaloy cladding. Lowry et al.[7,8] reported low-ductility (failure diametral strain $\lesssim 2\%$) failures of irradiated Zircaloy in internal-pressurization tube burst tests of Oconnee-I spent-fuel cladding (Table 5, Ref. 7) as well as in fast (strain rate ~0.1 to 0.001 s^{-1}) expanding-mandrel tests of Oconnee-I (Table 17 of Ref. 8) and H. B. Robinson spent-fuel cladding (Table 14 of Ref. 8). Both tests were conducted in an inert-gas environment. Bergenlid et al.[9] reported cladding cracks after a short power ramp and hold (total time $\lesssim 1.5$ min) in a test reactor following a base irradiation up to 25-29 MWd/kg U. Implications of these fuel rod failures observed under fast loading conditions have been discussed extensively in relation to rod failure probabilities during reactor off-normal events.[10]

B. TEM-Characterization of Ductile-Failure Specimens (H. M. Chung)

1. Introduction

It has been reported previously that irradiated cladding specimens that failed with minimal ductility in a PCI-like brittle manner were characterized by a very low dislocation density.[11] The dislocation entanglements were invariably observed in association with clusters of precipitates and irradiation-induced defects. In the dark-field contrasts, individual dislocations decorated by precipitates smaller than 10 nm in size could be observed. An s-parameter was defined as the fraction of the total number of selected area diffraction patterns (obtained from the dislocation entanglements) that contained the Zr_3O superlattice reflections. An s-parameter of ~0.6 was reported for a Big Rock Point specimen 165AE4B that failed in a brittle manner.[11] In this report, similar evaluation was conducted for a ductile Big Rock Point specimen 165AE4A. Ductile fracture surface morphology of the specimen was reported in Fig. 28 of Ref. 12.

2. Dislocation Characteristics

The small number of dislocations in brittle-type failure specimens, which are believed to be locked in by Zr_3O precipitates and irradiation-induced defect clusters, was observed only with the $\{002\}_\alpha$ of the α-matrix in strong reflection.[11] All images of the dislocation substructures listed in Table 2.1 of Ref. 11, which were obtained from the brittle-type failure specimen 165AE4B, showed such characteristics. In contrast to this, the dislocations in a ductile-failure specimen (e.g., Big Rock Point cladding specimen 165AE4A)[11] were observed in most cases with the $\{10\bar{1}0\}_\alpha$ or $\{0\bar{1}11\}_\alpha$ of the α-matrix reflections operating. An example is given in Fig. 2.3. A bright-field image and a selected area diffraction pattern are shown in Figs. 2.3(A) and (B), respectively. The Burgers vector of the dislocations is $\frac{1}{3}\vec{a}$ $\langle 11\bar{2}0\rangle$, indicating prism slip is involved. Thus, in the dark-field image of Fig. 2.3(C) produced with $(1\bar{1}00)_\alpha$, the dislocations are virtually invisible since $g\cdot b = 0$ (b the Burgers vector). However, the dislocations are visible in the $(10\bar{1}0)_\alpha$ dark-field image of Fig. 2.3(D) since $g\cdot b \neq 0$.

Dislocations characteristic of the brittle-failure specimens and observable with the $\{0002\}_\alpha$ reflections similar to Figs. 2.1 and 2.2 of Ref. 11 were also present in the ductile-failure specimen. However, such dislocations were relatively rare compared to the $\vec{a}$-component dislocations. For the 165AE4A specimen, out of a total of 31 selected areas examined for the characteristics of dislocations, only 5 areas were observed with the $\{0002\}_\alpha$ reflecting. The remaining 26 indicated prism-slip dislocations with the normal $\vec{a}$-component Burgers vector.

The dislocations observed with strong $\{0002\}_\alpha$ reflections are compatible with a Burgers vector containing a $\vec{c}$-component. Holt and Gilbert[13] reported similar dislocation characteristics for neutron irradiated Zircaloy-2 and concluded that the dislocations are indeed $\vec{c}$-component dislocations. However, their evidence should not be deemed conclusive since the possibility exists that the $\{0002\}$ reflections of the Zr_3O precipitates and the $\{002\}$ reflections of zirconium hydrides are operating. As shown in this work, those reflections are virtually superimposed on the $\{0002\}_\alpha$ reflections.[11]

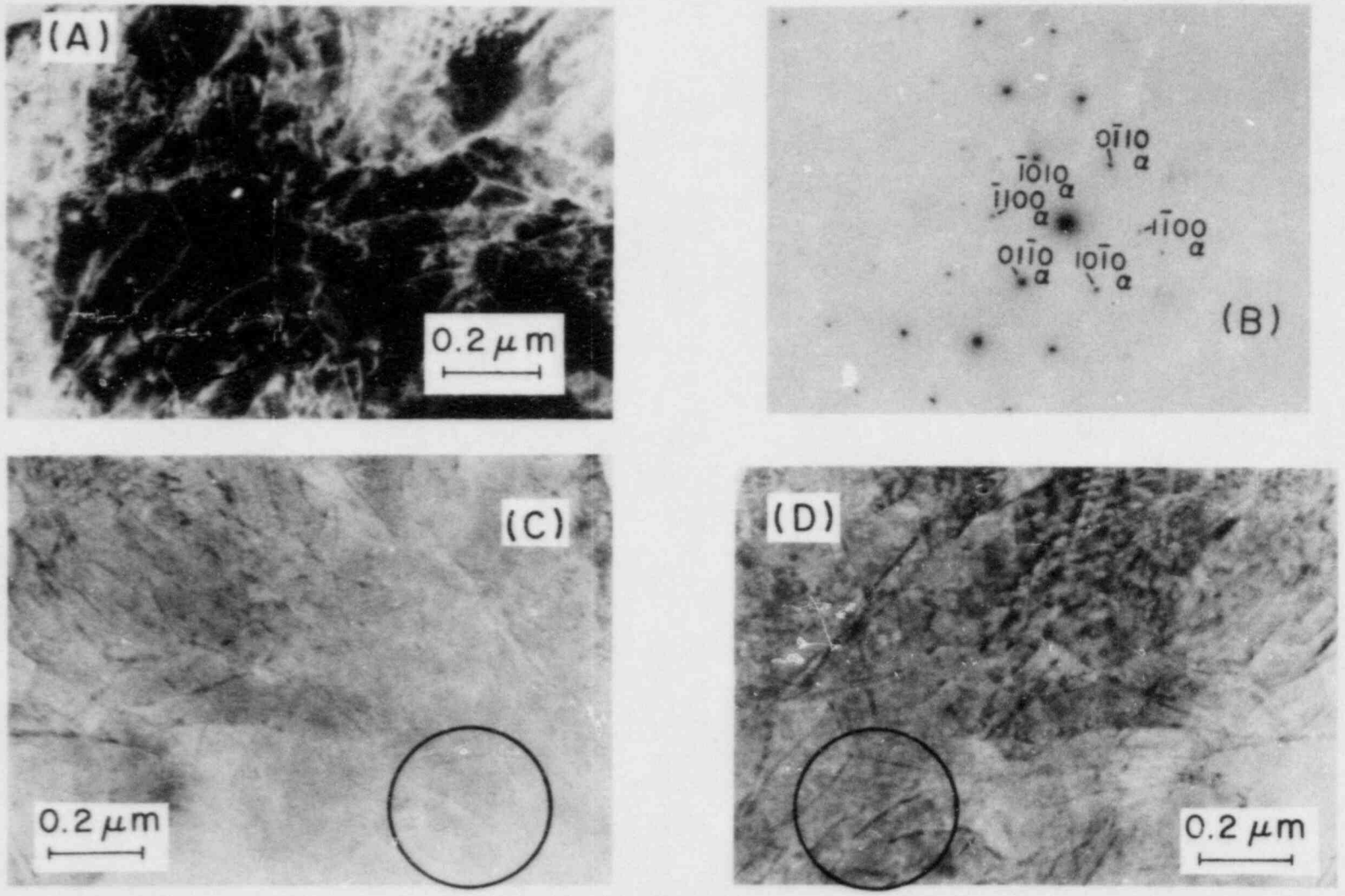

Fig. 2.3. Dislocation Structure in the Big Rock Point Cladding Specimen 1[illegible]5AE4A after a Ductile Fracture by Internal Gas Pressurization at 325°C. (A) Bright-field image; (B) indexed diffraction pattern of (A); (C) and (D) dark-field images of $(1\bar{1}00)_\alpha$ and $(0\bar{1}10)_\alpha$, respectively. Dislocation images are invisible in (C), indicating a prism slip with $\vec{a}$-component Burgers vector.

3. s-parameter of Ductile-Failure Specimen 165AE4A

A total of 31 dislocation substructures and corresponding selected-area diffraction patterns obtained from ductile-failure specimen 165AE4A were analyzed for the presence of Zr_3O superlattice reflections. The results are summarized in Table 2.1. Three patterns were found to contain the superlattice reflections. This results in an s-parameter of 0.09.

In comparison with an s-parameter of 0.61 previously reported for brittle-type failure specimen 165AE4B,[11] the result for ductile-failure specimen 165AE4A suggests negligible dislocation locking by the Zr_3O precipitates. As a consequence, a larger number of dislocation sources and mobile dislocations would be expected for specimen 165AE4A.

TABLE 2.1. Summary of TEM-HVEM Analysis of Zr_3O Superlattice Reflections Observed in Association with Dislocation Substructures in the Big Rock Point Spent-Fuel Cladding Specimen 165AE4A Which Failed in a Ductile Manner at 325°C by Internal Gas Pressurization[a]

Identification No. of Selected-Area Diffraction Pattern	Identification No. of Selected-Area Bright-Field Image[b]	Observed Zr_3O Superlattice Reflections[c]
35356	35355	None
35358	35357	None
35360	35359	None
35362	35361	None
35364	35363	None
35372	35371	None
35366	35365	None
35368	35367	$4\bar{4}\bar{3}$, $5\bar{3}\bar{2}$, $6\bar{2}\bar{1}$
35374	35373	103, 104, 105, 106, 107, $\bar{2}\bar{1}4$, $\bar{2}\bar{1}3$, $\bar{2}\bar{1}2$, $\bar{2}\bar{1}1$, $\bar{2}\bar{1}0$, $\bar{2}\bar{1}1$, $\bar{2}\bar{1}2$, $\bar{2}\bar{1}3$, $\bar{2}\bar{1}4$, $21\bar{2}$, $21\bar{1}$, 210, 211, 212

TABLE 2.1 (Contd.)

Identification No. of Selected-Area Diffraction Pattern	Identification No. of Selected-Area Bright-Field Image[b]	Observed Zr_3O Superlattice Reflections[c]
35379	35378	None
35370	35369	$\bar{3}\bar{1}2$, $\bar{2}03$, $\bar{1}14$
26675	26674	None
26670	26669	None
26651	26652	None
34169	34168	None
26658	26659	None
34178	34176	None
26666	26667	None
34180	34179	None
34783	34782	None
26743	26744	None
00038	00037	None
00041	00040	None
00045	00044	None
00056	00055	None
00066	00065	None
00019	00018	None
00022	00020	None
00027	00026	None
26980	26981	None
26988	26995	None

[a]For information on burnup, fluence, mechanical test conditions, SEM fractographic, and metallographic characteristics, see H. M. Chung, "TEM-HVEM Observation of Ordered Zirconium-Oxygen Phase in Zircaloy Spent-Fuel Cladding," Proc. Intl. Symp. on Environmental Degradation of Materials in Nuclear Power Systems-Water Reactors, Myrtle Beach, South Carolina, August 22-24, 1983, pp. 297-333.

[b]Bright-field image of the selected area containing the dislocation substructures.

[c]Denoted in Miller indices.

C. References for Chapter II

1. F. L. Yaggee, in Materials Science and Technology Division Ligh-Water-Reactor Safety Research Program: Quarterly Progress Report, July-September 1983, NUREG/CR-3689 Vol. III, ANL-83-85 Vol. III, pp. 24-28.
2. H. M. Chung, in Materials Science and Technology Division Light-Water-Reactor Safety Research Program: Quarterly Progress Report, October-December 1983, NUREG/CR-3689 Vol. IV, ANL-83-85 Vol. IV, pp. 113-123.
3. F. L. Yaggee, in Materials Science and Technology Division Light-Water-Reactor Safety Research Program: Quarterly Progress Report, April-June 1983, NUREG/CR-3689 Vol. II, ANL-83-85 Vol. II, pp. 98-114.
4. F. L. Yaggee, in Materials Science and Technology Division Light-Water-Reactor Safety Research Program: Quarterly Progress Report, April-June 1982, NUREG/CR-2970 Vol. II, ANL-82-41 Vol. II, pp. 79-96.
5. H. S. Rosenbaum, U. E. Wolff, and W. L. Bell, "Fractography of Incipient Cracks on Rod KE-2225," in Determination and Microscopic Study on Incipient Defects in Irradiated Power Reactor Fuel Rods, EPRI NP-812, July 1978, Electric Power Research Institute, pp. 3-97 to 3-141.
6. S. Ploger, "Trip Report on the First Information Survey by the Nuclear Regulatory Commission's Pellet-Cladding-Interaction Task force," Attachment to OGER-1-83, January 1983, EG&G Idaho, Inc.
7. L. M. Lowry, A. J. Markworth, J. S. Perrin, and M. P. Landow, Evaluating Strength and Ductility of Irradiated Zircaloy Task 5, Quarterly Progress Report, July-September 1979, NUREG/CR-1571, BMI-2057, Battelle Columus Laboratories.
8. L. M. Lowry, J. S. Perrin, A. J. Markworth, W. J. Gallager, ibid., July-December 1978, NUREG/CR-0981, BMI-2020.
9. U. Bergenlid, G. Lysell, H. Mogard, and G. Ronnberg, "The Studsvik Power Transient Programs DEMO-RAMP II and TRANS-RAMP I," Proc. Specialists' Meeting on Pellet Cladding Interaction in Water Reactor Fuel, October 3-5, 1983, Seattle, IWGFPT/18, International Atomic Energy Agency.
10. R. Van Houten, M. Tokar, and P. E. MacDonald, PCI-Related Cladding Failures During Off-Normal Events - DRAFT, NUREG/CR-3781, EGG-2313 DRAFT, May 1984, Draft Report of USNRC PCI Review Group.
11. H. M. Chung, in Materials Science and Technology Division Light-Water-Reactor Safety Fuel Systems Research Programs: Quarterly Progress Report, January-March 1984, NUREG/CR-3980 Vol. I, ANL-84-61 Vol. I, pp. 24-36.
12. H. M. Chung, in Materials Science and Technology Division Light-Water-Reactor Safety Research Program: Quarterly Progress Report, October-December 1981, NUREG/CR-2437 Vol. IV, ANL-81-77 Vol. IV, pp. 59-83.
13. R. A. Holt and R. W. Gilbert, "c-Component Dislocations in Neutron Irradiated Zircaloy-2," J. Nucl. Mater. 116, 127 (1983).

Distribution for NUREG/CR-3980 Vol. II (ANL-84-61 Vol. II)

Internal:

R. Avery
O. K. Chopra
H. M. Chung
L. W. Deitrich
C. E. Dickerman
G. R. Fenske
F. Y. Fradin
B. R. T. Frost
E. E. Gruber
G. L. Hofman
M. Ishii
W. D. Jackson
C. E. Johnson
T. F. Kassner (10)
K. L. Kliewer
J. M. Kramer
D. S. Kupperman
D. J. Lam
Y. Y. Liu
P. A. Lottes
P. S. Maiya
K. Natesan
L. A. Neimark
F. A. Nichols
P. R. Okamoto
R. G. Palm
J. Y. Park
R. B. Poeppel
L. E. Rehn
J. Rest (10)
W. E. Ruther
R. A. Scharping
W. J. Shack (3)
E. M. Stefanski (2)
R. V. Strain
C. E. Till
H. C. Tsai
R. A. Valentin
A. Villalobos
R. W. Weeks
H. Wiedersich
F. L. Yaggee
ANL Patent Dept.
ANL Contract File
ANL Libraries (3)
TIS Files (6)

External:

NRC, for distribution per R3 (275)
DOE-TIC (2)
Manager, Chicago Operations Office, DOE
R. Tom, DOE-CH
Materials Science and Technology Division Review Committee:
B. Alcock, U. Toronto
A. Arrott, Simon Fraser U.
R. C. Dynes, Bell Labs., Murray Hill
A. G. Evans, U. California, Berkeley
H. K. Forsen, Bechtel National, Inc., San Francisco
E. Kay, IBM San Jose Research Lab.
B. Maple, U. California, San Diego
P. G. Shewmon, Ohio State U.
J. K. Tien, Columbia U.
J. W. Wilkins, Cornell U.
R. B. Adamson, General Electric Co., Vallecitos Nuclear Center, P. O. Box 460, Pleasanton, Calif. 94566
P. L. Andresen, General Electric Corporate Research and Development, Schenectady, N. Y. 12301
G. A. Arlotto, Office of Nuclear Regulatory Research, USNRC, Washington
D. Atteridge, Battelle Pacific Northwest Lab., P. O. Box 999, Richland, Wash. 99352
D. L. Burman, Westinghouse PWR Systems Div., P. O. Box 355, Pittsburgh, Pa. 15230
L. K. Chan, Office of Nuclear Regulatory Research, USNRC, Washington
B. Cox, Chalk River Nuclear Labs., AECL, Chalk River, Ont., K0J 1J0, Canada
R. B. Foulds, Office of Nuclear Reactor Regulation, USNRC, Washington
S. M. Gehl, Electric Power Research Inst., P. O. Box 10412, Palo Alto, Calif. 94304
J. H. Gittus, Springfields Nuclear Power Development Labs., U. K. Atomic Energy Authority, Springfields, Salwick, Preston, PR4 ORR, England
R. R. Hobbins, EG&G/INEL, 1520 Sawtelle Dr., Idaho Falls, Idaho 83401
W. V. Johnston, Office of Nuclear Reactor Regulation, USNRC, Washington

R. L. Jones, Electric Power Research Inst., P. O. Box 10412, Palo Alto, Calif. 94304
K. R. Jordan, Nuclear Fuel Div., Monroeville Nuclear Center, Westinghouse Electric Corp., Monroeville, Pa. 15146
C. N. Kelber, Office of Nuclear Regulatory Research, USNRC, Washington
E. Kohn, Atomic Energy of Canada Ltd., Sheridan Park Research Community, Mississauga, Ont., Canada L5K 1B2
P. M. Lang, Office of Converter Reactor Deployment, USDOE, Washington, D. C. 20545
D. D. Lanning, Battelle Pacific Northwest Lab., P. O. Box 999, Richland, Wash. 99352
R. A. Lorenz, Oak Ridge National Lab., P. O. Box X, Oak Ridge, Tenn. 37830
P. MacDonald, EG&G/INEL, 1520 Sawtelle Dr., Idaho Falls, Idaho 83401
G. P. Marino, Office of Nuclear Regulatory Research, USNRC, Washington
S. McDonald, Westinghouse Electric Corp., R&D Center, Beulah Rd., Pittsburgh, Pa. 15235
K. R. Merckx, Exxon Nuclear, Inc., 2955 George Washington Way, Richland, Wash. 99352
A. C. Millunzi, Office of Nuclear Energy, USDOE, Washington, D. C. 20545
D. R. O'Boyle, Commonwealth Edison Co., P. O. Box 767, Chicago, Ill. 60690
R. N. Oehlberg, Electric Power Research Inst., P. O. Box 10412, Palo Alto, Calif. 94304
M. F. Osborne, Oak Ridge National Lab., P. O. Box X, Oak Ridge, Tenn. 37830
D. E. Owen, EG&G Idaho, P. O. Box 88, Middletown, Pa. 17057
T. P. Papazoglou, Lynchburg Research Center, Babcock & Wilcox Co., P. O. Box 1260, Lynchburg, Va. 24505
J. T. A. Roberts, Electric Power Research Inst., P. O. Box 10412, Palo Alto, Calif. 94304
H. H. Scott, Office of Nuclear Regulatory Research, USNRC, Washington
R. D. Silver, Office of Nuclear Reactor Regulation, USNRC, Washington
P. Smerd, Combustion Engineering, Inc., P. O. Box 500, Windsor, Conn. 06095
A. A. Solomon, School of Nuclear Engineering, Purdue U., West Lafayette, Ind. 47907
R. Van Houten, Office of Nuclear Regulatory Research, USNRC, Washington

NRC FORM 335 (11-81)

U.S. NUCLEAR REGULATORY COMMISSION

BIBLIOGRAPHIC DATA SHEET

1. REPORT NUMBER (Assigned by DDC)
NUREG/CR-3980 Vol. II
ANL-84-61 Vol. II

4. TITLE AND SUBTITLE (Add Volume No., if appropriate)
Light-Water-Reactor Safety Fuel Systems Research Programs: Quarterly Progress Report, April--June 1984

2. (Leave blank)

3. RECIPIENT'S ACCESSION NO.

7. AUTHOR(S)
J. Rest et al.

5. DATE REPORT COMPLETED
MONTH | YEAR

9. PERFORMING ORGANIZATION NAME AND MAILING ADDRESS (Include Zip Code)
Argonne National Laboratory
9700 South Cass Avenue
Argonne, Illinois 60439

DATE REPORT ISSUED
MONTH | YEAR
February 1935

6. (Leave blank)

8. (Leave blank)

12. SPONSORING ORGANIZATION NAME AND MAILING ADDRESS (Include Zip Code)
Division of Accident Evaluation
Office of Nuclear Regulatory Research
U. S. Nuclear Regulatory Commission
Washington, D. C. 20555

10. PROJECT/TASK/WORK UNIT NO.

11. FIN NO.
A2016, A2017

13. TYPE OF REPORT
Technical

PERIOD COVERED (Inclusive dates)
April--June 1984

15. SUPPLEMENTARY NOTES

14. (Leave blank)

16. ABSTRACT (200 words or less)

This progress report summarizes the Argonne National Laboratory work performed during April, May, and June 1984 on water reactor safety problems related to fuel and fuel cladding materials. The research and development areas covered are Transient Fuel Response and Fission Product Release and Clad Properties for Code Verification.

17. KEY WORDS AND DOCUMENT ANALYSIS

17a. DESCRIPTORS

fission product modeling
fission product release
irradiated Zircaloy cladding
mandrel loading tests
Zircaloy fracture
Zr_3O precipitation

17b. IDENTIFIERS/OPEN-ENDED TERMS

18. AVAILABILITY STATEMENT
Unlimited

19. SECURITY CLASS (This report)
unclassified

21. NO. OF PAGES
32

20. SECURITY CLASS (This page)
unclassified

22. PRICE
$

NRC FORM 335 (11-81)